Experimental Demonstration of Self-Collimation inside a Three-Dimensional Photonic Crystal

Zhaolin Lu, Shouyuan Shi, Janusz A. Murakowski, Garrett J. Schneider, Christopher A. Schuetz, and Dennis W. Prather

Department of Electrical and Computer Engineering, University of Delaware, Newark, Delaware 19716, USA

(Received 15 December 2005; published 4 May 2006)

We present our experimental demonstration of self-collimation inside a three-dimensional (3D) simple cubic photonic crystal at microwave frequencies. The photonic crystal was designed with unique dispersion property and fabricated by a high precision computer-controlled machine. The self-collimation modes were excited by a grounded waveguide feeding and detected by a scanning monopole. Self-collimation of electromagnetic waves in the 3D photonic crystal was demonstrated by measuring the 3D field distribution, which was shown as a narrow collimated beam inside the 3D photonic crystal but a diverged beam in the absence of the photonic crystal.

DOI: 10.1103/PhysRevLett.96.173902 PACS numbers: 42.70.Qs, 42.25.Bs, 42.79.Gn, 78.20.−e

Electromagnetic beams diverge when propagating in dielectric materials due to diffraction. It seems to be a rule of thumb that no material can sustain and preserve the size of a narrow beam unless specific structural routes (e.g., waveguides, index gradients, or line defects) are incorporated. Recently, the development of photonic crystals (PhCs) has enabled ground breaking approaches to control the flow of electromagnetic waves. Many applications of PhCs stem from the existence of a photonic bandgap (PBG) in a certain frequency range, where no electromagnetic wave is permitted to propagate. If defects are introduced in PBG materials, localized modes can be excited. The localized modes can be either cavity modes for point defects [1] or guiding modes for linear defects [2]. In this sense, PBG provides a powerful guiding approach since the guiding route, which depends on the defects incorporated in the PhC, can be extremely narrow and sharply bent [1]. On the other hand, recently substantial interest has arisen in the unique dispersion properties provided by PhCs [3,4]. Unique dispersion-related phenomena include negative refraction [5,6], superprism [7], and slowing light [8]. Another dispersion-related phenomenon for PhCs is self-collimation [9,10]. When a PhC works in a self-collimation mode, an electromagnetic beam can propagate within it without divergence. In other words, an electromagnetic wave propagates as if there were no diffraction in the material. Self-collimation in two-dimensional (2D) PhCs has recently been demonstrated [4,9,11,12], providing an innovative guiding approach, where nevertheless the vertical confinement of light is still achieved by index guidance. Numerical investigations of self-collimation in 3D PhCs were firstly reported in Refs. [13,14], and recently in Refs. [15,16], offering tantalizing new evidence that self-collimation in 3D PhCs should be possible, and opening the door to producing a totally new category of materials, namely, ''nondiffractive materials.'' However, no experimental work has been reported to date. The challenges are mostly attributable to the difficulty of 3D structure fabrication, and 3D field distribution measurement. As far as we know, there has never been experimental work reported to measure field distribution inside a 3D PhC at all. In our work, we have overcome these challenges. Herein, we demonstrate a 3D PhC as a new material, in which light can propagate without divergence while no specific route is introduced. A 3D PhC with desired dispersion was fabricated, and self-collimation was experimentally verified by mapping the field distribution *inside* the volume of the 3D PhC.

Figure 1(a) shows the 3D PhC we employed in this work. It is a simple cubic lattice with the unit cell shown in the inset. The hole diameter is $2r = 3.2$ mm, the lattice constant is $a = 5.0$ mm, and the microwave material has a dielectric constant $\varepsilon_r = 30$ (HiK500F, obtained from Emerson & Cumming). The overall dimensions are $W85$ mm $\times$ $H76$ mm $\times$ $L170$ mm. The propagation of electromagnetic waves in a PhC is governed by Maxwell equations with the periodic boundary condition defined by the PhC structure. In designing the structure, we used a plane-wave expansion method [17] to solve the Maxwell equations and obtain the eigenvalues of frequency f for a given wave vector $\mathbf{k}$. Figure 1(b) shows the f-$\mathbf{k}$ diagram around the perimeter of the irreducible first Brillouin zone, also called the photonic band diagram. According to the diagram, a small band gap appears between 14.4 and 15.0 GHz, but that is not our center of attention. Instead, we focus on a frequency region centered at 12.3 GHz, where self-collimation is expected. Figure 2(a) shows the equi-frequency surfaces (EFSs) [10] at 12.3 GHz. Notice that the EFSs are depicted in k space and two degenerate bands exist. The third band (red online) is located inside the fourth band (blue online). The third band is also depicted separately in Fig. 2(b). Since group velocity (and hence the direction of power flow) is calculated by the gradient of frequency in k space, i.e., $\mathbf{v}_g = 2\pi\nabla_k f(\mathbf{k})$, power propagation direction is perpendicular to the EFSs. Although two bands are degenerate, both EFSs are nearly flat and, hence, 3D self-collimation modes are possibly supported.

To understand this in depth, we consider a beam propagates along the z axis and express the field distribution in

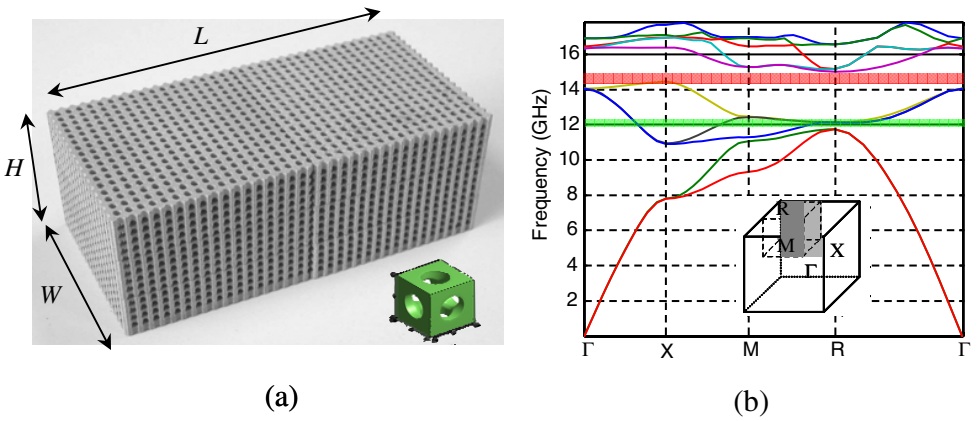

FIG. 1 (color online). (a) The simple cubic PhC fabricated by a high precision computer-controlled machine. It has $18 \times 15 \times 36$ units. $W = 85$ mm, $H = 76$ mm, and $L = 170$ mm. (b) The photonic band diagram for the PhC.

k space as $A(k_x, k_y; z = 0)$. Propagation along the z axis will increase the phase for each k component, and the field distribution at $z = L$ is $A(k_x, k_y; z = L) = A(k_x, k_y; z = 0)\exp(ik_z L)$. In most cases, k_z is the function of k_x and k_y as, for example, $k_z(k_x, k_y) = \sqrt{\varepsilon_r k_0^2 - (k_x^2 + k_y^2)}$ in a common isotropic material. So the propagation gives rise to different phase growths for different k components. The result is diffraction. The uniqueness of the PhC lies in its dispersion governed by $k_z(k_x, k_y) \approx$ constant in a certain frequency range. So the phase growth due to propagation is independent of (k_x, k_y) and, hence, the field distribution is *frozen*. If the original field carries an image, the image with the *same size* can be retrieved anywhere along the propagation direction. One direct result is the maintenance of the beam size, i.e., self-collimation.

Closer examination of the EFSs shows that EFS for the third band is flat in the middle (lower $|k|$) and slightly curved at the edges (higher $|k|$), while the fourth band is slightly curved in the middle and flat at the edges; see Fig. 2(c). Because most energy of a propagation beam is concentrated at lower $|k|$ components, better self-collimation modes are expected to be excited at the third band. Three-dimensional finite-difference time-domain simulations showed that these two degenerate bands are strongly polarization dependent in the simple cubic structure. In particular, magnetic current sources will excite self-collimation modes at the third band, while electric current sources will excite modes at the fourth band [13].

A high precision computer-controlled machine was employed to fabricate devices for microwave and millimeter-wave applications [5,6,11]. This 3D simple cubic PhC was fabricated by drilling aligned holes along the three orthogonal axes in six 85 mm $\times$ 85 mm $\times$ 25 mm pieces of the dielectric material. These pieces were aligned and stacked to form the complete PhC. The fabrication precision was controlled to ± 0.1 mm, which is very small compared with the lattice constant and the wavelength of electromagnetic waves we will use. To perform the experiment, we established a 3D microwave imaging system [18]. The detector, a monopole 1.8 mm in diameter with a 1 mm length of core exposed at the end, was mounted on an XYZ scanner. The fixed source was a waveguide with a flat copper ground plane (with an aperture 1 cm by 1 cm) at the end, and electric component polarized along the verti-

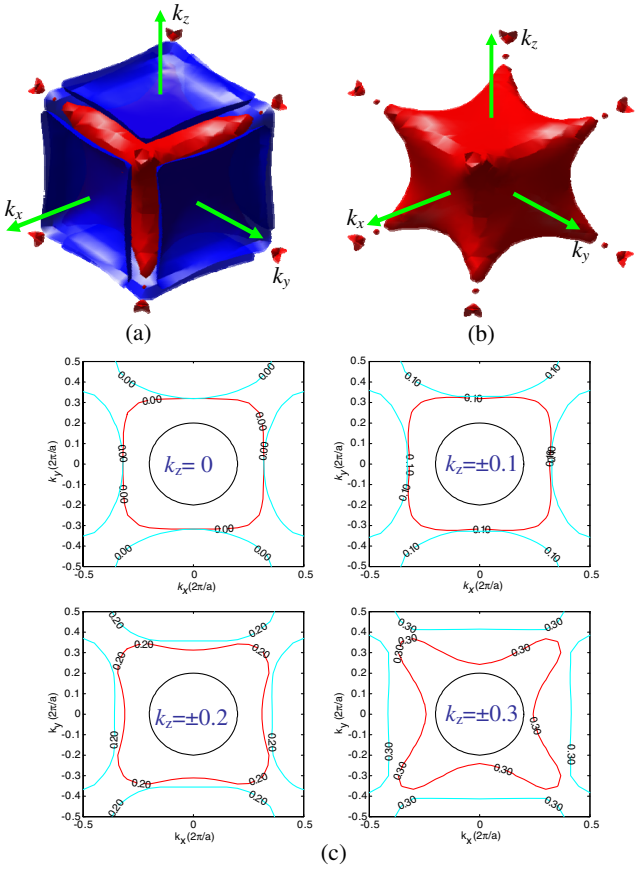

FIG. 2 (color online). (a) The equi-frequency surfaces for frequency $f = 12.3$ GHz. The third and fourth bands are degenerate. (b) The equi-frequency surface of the third band. (c) The equi-frequency surfaces shown as a series of contours for different k_z components. The black circle on each diagram is the dispersion contour for air.

cal axis. This configuration of the source is equivalent to a magnetic dipole source [19], which can excite the self-collimation modes in the third band. The source and the detector were connected to a vector network analyzer, through which the electric field distribution can be measured at any given point. A custom program was developed to synchronize the motion of the detector and the measurement of the corresponding field distribution. The diameter of the detector (1.8 mm) is smaller than that of the holes (3.2 mm). So we can insert the detector into the holes to map the field distribution inside all holes of the PhC following a point-by-point and hole-by-hole process. The presence of the detector introduces a defect, which will disturb the guiding route defined by linear boundaries, e.g., defect-guiding. However, in our case the guiding route is defined by the widely spreading periodicity of the PhC. Its influence on the field distribution is negligible. This is also verified by the experimental results presented in the following text.

In our experiment, we varied the frequency from 11.0 to 17.0 GHz at intervals of 0.1 GHz, and measured the electric field at 75 points along the length of each hole separated by 1.0 mm steps. As a result, the electric field amplitude distribution was obtained as a 3D matrix with $X75 \times Y17 \times Z34$ elements for each frequency. To estimate the beam size within the PhC, we used a standard definition of full width at half maximum (FWHM), where we reduced the effect of random variation by averaging the five highest values in each xy slice as the reference maximum value of that slice. To show the change of the beam size along the propagation direction, we determined the half maximum of the intensity in each xy slice along the z axis and rendered all of the half-maximum intensity contours as a 3D surface. As a result, the beam profile along the length of the PhC is indicated by the enclosed part of the 3D surface. Figure 3(a) shows the beam profile at $f = 12.2$ GHz, which is a narrow, collimated beam. The first movie in Ref. [20] illustrates how the beam evolves in space and also shows the intensity distribution on each slice along the z axis. The intensity distributions of slices located at $z = 15$ mm and $z = 165$ mm are also shown in the left and right insets of Fig. 3(a), respectively. We calculated the beam diameters on all slices along the z axis, and depicted them in Fig. 3(b). Curve fitting shows that the diameter of the beam increases 2 mm (from 8.5 to 10.5 mm) at the propagation distance of 165 mm. Close examination reveals the increase is mostly due to a jump at $z = 80$ mm, where considerable lattice misalignment exists. Optimizing the fabrication accuracy will improve the self-collimation. In contrast, at the same propagation distance a Gaussian beam [21] (with the waist size = 8.5 mm) theoretically expands its waist into 150 mm in the air and 29 mm in a material with $\varepsilon_r = 30$, which are shown in Fig. 3(b) (shown online as red and blue curves, respectively).

Detailed analysis demonstrated that this self-collimation phenomenon was observed in the frequency range 12.1–12.9 GHz, consistent with the flat EFSs calculated for the

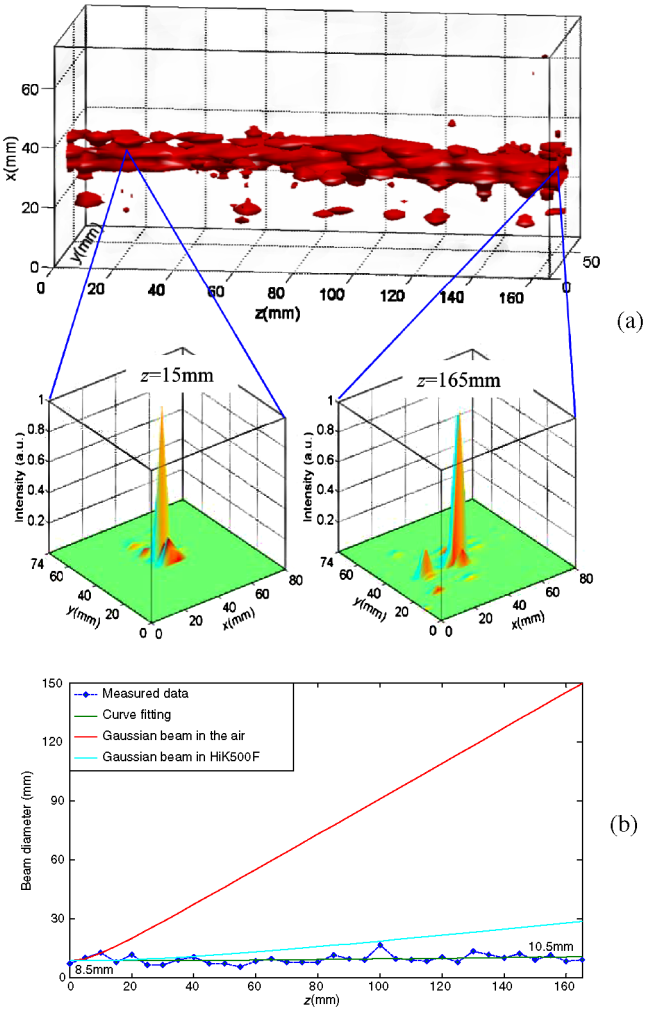

FIG. 3 (color online). (a) The FWHM beam profile in the PhC at $f = 12.2$ GHz. (b) The evolution of beam diameter in the PhC and common materials.

third dispersion band at these frequencies. The second movie in Ref. [20] shows how the beam profile changes as a function of frequency. For comparison, we repeated the same measurement and analysis for the electromagnetic wave propagation in the air by removing the PhC while keeping all other instruments and their states. The third movie in Ref. [20] shows a divergent beam profile in the air when the source is set at $f = 12.2$ GHz. The discrepancy of the profiles from ideal divergent beams is due to the reflection from environments. No collimated beam in the air is observed at any frequency in the range we measured. Therefore, the comparison of Fig. 3(a) with the third part of Ref. [20] further confirms that it is the presence of 3D PhC that results in the collimation of electromagnetic beam. In other words, the PhC cancels the diffraction effect and functions as a nondiffractive material.

To observe how power is transported inside the PhC, we integrated the intensity over the first xy slice and used it as input power, and the last slice as output power. The propa-

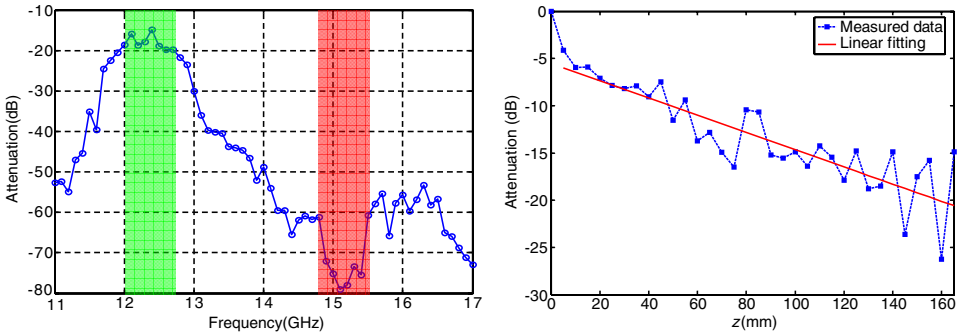

FIG. 4 (color online). (a) The relationship between the attenuation and working frequency. (b) The attenuation along the z axis at $f = 12.4$ GHz.

gation attenuation in the PhC can be calculated as the ratio between output and input. For different frequencies, we obtained different attenuations. Figure 4(a) shows the relationship between the attenuation and frequency. From this diagram, one can see that the largest attenuation (79 dB) occurs inside bandgap (15.1 GHz) while the smallest attenuation (15 dB) occurs when the beam is self-collimated (12.4 GHz). The left and right (green and red online) shaded bars indicate the minimum and maximum attenuation regions, respectively, which also coincide with the self-collimation and bandgap ranges, respectively. In bandgap ranges, most of power dies out in the first several lattices. In the self-collimation, the power (in dB) decays approximately linearly along the z axis, as shown in Fig. 4(b), except for considerable insertion loss in the coupling process. Similar issue also occurs in 2D self-collimation which was reported in Ref. [12]. This may be solved by index matching or other novel approaches.

In conclusion, a 3D simple cubic PhC was fabricated and its dispersion properties were investigated. Experiments demonstrated 3D self-collimation in the PhC by mapping 3D field distribution inside the PhC. Owing to the advances in the fabrication of nanoscale PhCs [22], similar materials are expected to emerge for light-wave applications to address a series of challenges, such as high-density optical interconnects and low optical-channel crosstalk.

[1] S. Y. Lin, E. Chow, V. Hietala, P. R. Villeneuve, and J. D. Joannopoulos, Science **282**, 274 (1998).
[2] S. Ogawa, M. Imada, S. Yoshimoto, M. Okano, and S. Noda, Science **305**, 227 (2004).
[3] S. Y. Lin, V. M. Hietala, L. Wang, and E. D. Jones, Opt. Lett. **21**, 1771 (1996).
[4] D. W. Prather, S. Shi, D. M. Pustai, C. Chen, S. Venkataraman, A. Sharkawy, G. J. Schneider, and J. A. Murakowski, Opt. Lett. **29**, 50 (2004).
[5] Z. Lu, J. A. Murakowski, C. A. Schuetz, S. Shi, G. J. Schneider, and D. W. Prather, Phys. Rev. Lett. **95**, 153901 (2005).
[6] Z. Lu, C. Chen, C. A. Schuetz, S. Shi, J. A. Murakowski, G. J. Schneider, and D. W. Prather, Appl. Phys. Lett. **87**, 091907 (2005).
[7] H. Kosaka, T. Kawashima, A. Tomita, M. Notomi, T. Tamamura, T. Sato, and S. Kawakami, Phys. Rev. B **58**, R10096 (1998).
[8] M. Soljacic, S. G. Johnson, S. Fan, M. Ibanescu, E. Ippen, and J. D. Joannopoulos, J. Opt. Soc. Am. B **19**, 2052 (2002).
[9] H. Kosaka, T. Kawashima, A. Tomita, M. Notomi, T. Tamamura, T. Sato, and S. Kawakamib, Appl. Phys. Lett. **74**, 1212 (1999).
[10] J. Witzens, M. Loncar, and A. Scherer, IEEE J. Sel. Top. Quantum Electron. **8**, 1246 (2002).
[11] Z. Lu, C. A. Schuetz, S. Shi, C. Chen, G. P. Behrmann, and D. W. Prather, IEEE Trans. Microwave Theory Tech. **53**, 1362 (2005).
[12] P. T. Rakich *et al.*, Nat. Mater. **5**, 93 (2006).
[13] D. W. Prather, S. Shi, S. Venkataraman, Z. Lu, J. Murakowski, and G. Schneider, Proc. SPIE Int. Soc. Opt. Eng. **5733**, 84 (2005).
[14] D. W. Prather, S. Venkataraman, S. Shi, G. Schneider, and J. Murakowski, Proc. SPIE Int. Soc. Opt. Eng. **5595**, 45 (2004).
[15] J. Shin and S. Fan, Opt. Lett. **30**, 2397 (2005).
[16] R. Iliew, C. Etrich, and F. Lederer, Opt. Express **13**, 7076 (2005).
[17] S. G. Johnson and J. D. Joannopoulos, Opt. Express **8**, 173 (2001).
[18] Z. Lu, S. Shi, C. A. Schuetz, J. A. Murakowski, and D. W. Prather, Opt. Express **13**, 5592 (2005).
[19] C. A. Balanis, *Advanced Engineering Electromagnetics* (John Wiley & Sons, Inc, New York, 1989), p. 334.
[20] See EPAPS Document No. E-PRLTAO-96-025620 for movies of the evolution of the beam profile. For more information on EPAPS, see http://ww.aip.org/pubservs/epaps.html.
[21] See, for example, B. A. Saleh and M. C. Teich, *Fundamentals of Photonics* (John Wiley & Sons, Inc., New York, 1991), pp. 80–107.
[22] P. Yao, G. J. Schneider, B. Miao, J. Murakowski, and D. W. Prather, Appl. Phys. Lett. **85**, 3920 (2004).